Journal of Porphyrins and Phthalocyanines
J. Porphyrins Phthalocyanines 2012; **16**: 518–529
DOI: 10.1142/S1088424612500460

Formation and characterization of five- and six-coordinate iron(III) corrolazine complexes

Satoshi Kurahashi[b◊◊], **Takahisa Ikeue***[a◊], **Tamotsu Sugimori**[c], **Masashi Takahashi**[d,e], **Masahiro Mikuriya**[b], **Makoto Handa**[a◊], **Akira Ikezaki**[f◊] **and Mikio Nakamura***[e,f,g◊]

[a] *Department of Material Science, Interdisciplinary Faculty of Science and Engineering, Shimane University, 1060 Nishikawatsu, Matsue 690-8504, Japan*
[b] *Department of Chemistry and Research Center for Coordination Molecule-Based Devices, School of Science and Technology, Kwansei Gakuin University, 2-1 Gakuen, Sanda 669-1337, Japan*
[c] *Division of Chemistry, Graduate School of Medicine and Pharmaceutical Sciences, University of Toyama, Toyama 930-0194, Japan*
[d] *Department of Chemistry, Faculty of Science, Toho University, Funabashi 274-8510, Japan*
[e] *Research Center for Materials with Integrated Properties, Toho University, Funabashi 274-8510, Japan*
[f] *Department of Chemistry, School of Medicine, Toho University, Ota-ku, Tokyo 143-8540, Japan*
[g] *Division of Chemistry, Graduate School of Science, Toho University, Funabashi 274-8510, Japan*

Dedicated to Professor Emanuel Vogel in memoriam

Received 28 September 2011
Accepted 21 November 2011

ABSTRACT: Electronic structures of five- and six-coordinate iron(III) corrolazine complexes are determined by means of ^{1}H NMR, ^{13}C NMR, EPR, and Mössbauer spectroscopy as well as SQUID magnetometry. A series of five-coordinate complexes, $[Fe^{III}(TBP_8Cz)(L)]$* where the axial ligands(L) are cyanide(CN^-), imidazole(HIm), 1-methylimidazole(1-MeIm), 4-(*N*,*N*-dimethylamino)pyridine(DMAP), pyridine(Py), 4-cyanopyridine(4-CNPy), and *tert*-butylisocyanide(^{t}BuNC), are obtained by the addition of 1 to 2 equiv. of the ligands to the dichloromethane solutions of $Fe^{III}(TBP_8Cz)$ at 298 K: TBP_8Cz is a trianion of 2,3,7,8,12,13,17,18-octakis(4-*tert*-butylphenyl)corrolazine. These complexes commonly show the S = 3/2 at 298 K. By contrast, formation of the six-coordinate complexes depends on the nature of the axial ligands. While the addition of 3 equiv. of CN^- has completely converted $Fe^{III}(TBP_8Cz)$ to $(Bu_4N)_2[Fe^{III}(TBP_8Cz)(CN)_2]$ at 298 K, the conversion to the bis-adduct is only attained below *ca*. 200 K in the case of HIm, 1-MeIm, and DMAP even in the presence of 50 equiv. of the ligands. If the axial ligand is Py, 4-CNPy, or ^{t}BuNC, the formation of $[Fe^{III}(TBP_8Cz)(L)_2]$ is confirmed only at an extremely low temperature (15 K). Close inspection of the ^{1}H NMR and EPR spectra has revealed that all the bis-adducts adopt the $(d_{xy})^2(d_{xz}, d_{yz})^3$ ground state. While $Fe^{III}(TBP_8Cz)$ forms paramagnetic bis- and mono-adduct in toluene solution at 298 K in the presence of excess amount of CN^- and ^{t}BuNC, respectively, the corresponding porphyrazine complex, $[Fe^{III}(TBP_8Pz)]Cl$, forms diamagnetic bis-CN and bis-^{t}BuNC under the same conditions: TBP_8Pz is a dianion of 2,3,7,8,12,13,17,18-octakis(4-*tert*-butylphenyl)-porphyrazine. Thus, the iron(III) ion of porphyrazine complex is more easily reduced than that of the corresponding corrolazine complex.

KEYWORDS: corrolazine, iron(III) complexes, spin state, electron configuration.

◊SPP full and ◊◊student member in good standing

*Correspondence to: Takahisa Ikeue, email: ikeue@riko.shimane-u.ac.jp and Mikio Nakamura, email: mnakamu@med.toho-u.ac.jp

INTRODUCTION

Electronic structures of iron(III) porphyrin complexes can be modulated by various factors which include the field strength of the axial ligand, electronic effect of the peripheral substituent, deformation of the porphyrin ring, hydrogen bonding to the axial ligand, etc. [1–3]. By manipulating these factors, we are now able to obtain various iron(III) complexes with different electronic structures, *i.e.* S = 1/2 with the $(d_{xy})^2(d_{xz}, d_{yz})^3$, S = 1/2 with the $(d_{xz}, d_{yz})^4(d_{xy})^1$, S = 3/2 with the $(d_{xy})^2(d_{xz}, d_{yz})^2(d_{x^2})^1$, and S = 3/2 with the $(d_{xz}, d_{yz})^3(d_{xy})^1(d_{x^2})^1$ [4–8]. As an extension of our on going studies on determining the factors that control the electronic structure of iron(III) porphyrins, we have expanded the system from the porphyrins to the porphyrin analogues. Such studies have revealed that iron(III) porphycene core stabilizes the S = 3/2 state as compared with other iron(III) complexes of the corresponding porphyrin and porphyrin isomers such as corrphycene and hemiporphycene [9–12]. As is well known, the chemistry of these porphyrin isomers has been developed by the pioneering work of the late Prof. Vogel and others [13–21]. Not only the spin states, but also the electron configuration of low-spin complexes is perturbed by the core modification. For example, the chlorin core stabilizes the $(d_{xz}, d_{yz})^4(d_{xy})^1$ ground state as compared with the corresponding porphyrin core [22–25]. In contrast, replacement of the *meso*-carbon atoms by one or two nitrogen atoms greatly stabilizes the $(d_{xy})^2(d_{xz}, d_{yz})^3$ ground state. Thus, the six-coordinate S = 1/2 complexes of substituted monoazaporphyrin (H_2MAzP) and diazaporphyrin (H_2DAzP) such as $[Fe^{III}(MAzP)(L)_2]^{\pm}$ (1) and $[Fe^{III}(DAzP)(L)_2]^{\pm}$ (2) shown in Chart 1 adopt the $(d_{xy})^2(d_{xz}, d_{yz})^3$ ground state even if the axial ligand(L) is ^{t}BuNC [26, 27]. The result is quite unusual since almost all the low-spin iron(III) complexes reported previously adopt the $(d_{xz}, d_{yz})^4(d_{xy})^1$ electronic ground state if the axial ligand is ^{t}BuNC [27−29]. We have also found that the ^{13}C NMR chemical shifts of the pyrrole-C_α signals in substituted porphyrazine $H_2(TBP_8Pz)$ complexes such as five-coordinate $Fe^{III}(TBP_8Pz)X$ (X = Cl^-, Br^-, and I^-) and six-coordinate $[Fe^{III}(TBP_8Pz)(L)_2]^*$ (3) shown also in Scheme 1 are the excellent probe to determine the subtle change in the spin state and electron configuration of the iron(III) ions, where the ^{1}H NMR chemical shifts are less useful because of the absence of the *meso*-carbon atoms [30]. Recently, Goldberg and co-workers have disclosed the synthesis of corrolazine, $H_3(TBP_8Cz)$, a new member of the porphyrinoid family having triazacorrole structure, and have extensively studied the catalytic activities of its manganese and iron complexes, *i.e.* $Mn^{III}(TBP_8Cz)$ and $Fe^{III}(TBP_8Cz)$ [31–42]. We are very much interested in the electronic ground state of the iron(III) complexes of this new porphyrinoid. In this paper, we will describe the formation and electronic structures of a series of five- and six-coordinate $[Fe^{III}(TBP_8Cz)(L)]^*$ and $[Fe^{III}(TBP_8Cz)\text{-}(L)_2]^*$(4) carrying typical nitrogen bases such as HIm, 1-MeIm, DMAP, Py, and 4-CNPy as well as carbon bases such as CN^- and ^{t}BuNC by means of UV-vis, ^{1}H NMR, ^{13}C NMR, Mössbauer, EPR spectra, and SQUID measurement. The electronic structures of the corrolazine complexes (4) are compared with those of the corresponding porphyrazine complexes (3).

EXPERIMENTAL

Measurements

UV-vis spectra were recorded for the CH_2Cl_2 solutions from 300 to 900 nm on a Shimazu UV-3100 spectrophotometer. The UV-vis spectra at low temperatures were recorded from 300 to 800 nm on a Shimadzu MultiSpec-1500 spectrophotometer equipped with a UNISOKU liquid nitrogen cryostat, CoolSpec UV USP-203-A. ^{1}H and ^{13}C NMR spectra were recorded either on a JEOL LA 400 spectrometer operating at 400.1 MHz or on a JEOL ECS-500SS spectrometer operating at 500.0 MHz for ^{1}H. Chemical shifts were referenced to the residual peaks of CD_2Cl_2(δ = 5.32 and 52.3 ppm for the ^{1}H and ^{13}C signals, respectively). EPR spectra were recorded in frozen toluene solution at 15 K on a Bruker E500 spectrometer operating at X band and equipped with an Oxford helium cryostat. Some samples were measured in frozen CH_2Cl_2 solution or in the solid. Iron-57 Mössbauer spectra were measured on a Wissel Mössbauer spectrometer system consisting of an MDU-1200 function generator, a DFG-1200 driving unit, and an MVT-100 velocity transducer, incorporating with a

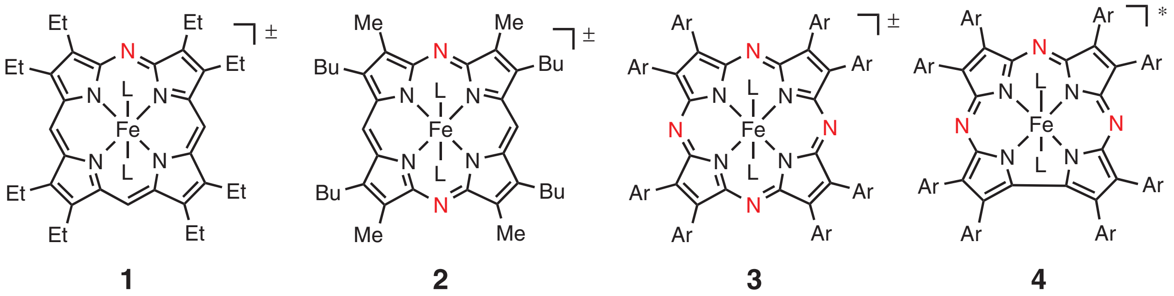

Chart 1. Six-coordinate iron(III) complexes of monoazaporphyrin(MAzP) (**1**), diazaporphyrin(DAzP) (**2**), tetraazaporphyrin or porphyrazine(Pz) (**3**), and triazacorrole or corrolazine(Cz) (**4**)

model 7800 multichannel analyzer form Seiko EG&G Co. Ltd. The samples were kept in a Heli-Tran LT-3 gas-flow cryostat from Advanced Research System Inc. equipped with a 9620 digital temperature controller from Scientific Instruments Inc., and the ^{57}Co(Rh) source was kept at room temperature. The data were analyzed on a MossWinn 3.0 i Software. The isomer shift is given relative to α-iron foil at room temperature. MALDI-TOF-MS spectra were recorded on a Bruker Daltonics pAutoflex-T1. The solid state magnetic susceptibilities were measured over the temperature range 4.5–300 K in a magnetic field of 0.5 T with a SQUID magnetometer (Quantum Design MPMS). The measured data were corrected for diamagnetic contributions. The effective magnetic moment (μ_1^{eff}) of [Fe$^{\text{III}}$(TBP$_8$Cz)(L)]* was determined in solution relative to that of intermediate-spin Fe$^{\text{III}}$(TBP$_8$Cz) ($\mu_2^{\text{eff}} = 3.89\ \mu_B$) by the Evans method [43], using CH$_2$Cl$_2$ as the chemical shift reference according to the following equation; $\mu_1^{\text{eff}} = (\Delta\nu_1/\Delta\nu_2)^{1/2}\mu_2^{\text{eff}}$ [44]. In this equation, $\Delta\nu_1$ and $\Delta\nu_2$ are the differences in chemical shifts of CH$_2$Cl$_2$ in [Fe$^{\text{III}}$(TBP$_8$Cz)-(L)]* and Fe$^{\text{III}}$(TBP$_8$Cz), respectively. The effective magnetic moments of [Fe$^{\text{III}}$(TBP$_8$Cz)(L)$_2$]* were similarly determined.

Synthesis

H$_3$(TBP$_8$Cz). Free-base corrolazine was prepared from the corresponding porphyrazine H$_2$(TBP$_8$Pz) [45], *via* phosphrous corrolazine [P(TBP$_8$Cz)OH](OH), according to the method developed by Goldberg and co-workers [31, 46]. Since the solvents used for the NMR and UV-vis measurements are different from those reported by Goldberg and co-workers, the chemical shifts and absorption maxima are given below. ^{1}H NMR (400 MHz; CD$_2$Cl$_2$; 298 K): δ_H, ppm 8.21 (4H, br s), 8.11 (4H, br s), 7.80 (4H, br s), 7.67 (4H, d, $J_{H\text{-}H}$ = 7.3 Hz), 7.65 (4H, d, $J_{H\text{-}H}$ = 7.9 Hz), 7.51 (4H, d, $J_{H\text{-}H}$ = 8.2 Hz), 7.44 (4H, d, $J_{H\text{-}H}$ = 8.2 Hz), 7.16 (4H, d, $J_{H\text{-}H}$ = 8.2 Hz), 1.49 (18H, s), 1.48 (18H, s), 1.42 (18H, s), 1.34 (18H, s). MALDI-TOF MS: *m/z* 1358.84 (calcd. for C$_{96}$H$_{107}$N$_7$ 1358.92). UV-vis (CHCl$_3$): λ_{max}, nm (ε 10^4 M^{-1}.cm^{-1}) 465 (8.58), 625 (1.97), 686 (3.94). IR (KBr): ν, cm^{-1} 3359, 2960, 2903, 2867, 2356, 1476, 1459, 1393, 1361, 1267, 1213, 1107, 982, 969, 836, 772, 739, 565. Anal. calcd. for C$_{96}$H$_{107}$N$_7$: C, 84.85; H, 7.94; N, 7.22%. Found: C, 84.35; H, 7.59; N, 7.08.

[P$^{\text{V}}$(TBP$_8$Cz)(OH)]OH(^{13}C$_\alpha$). Phosphorus corrolazine complex where pyrrole-C$_\alpha$ is ^{13}C enriched was prepared by the reaction between PBr$_3$ and H$_2$(TBP$_8$Pz) (^{13}C$_\alpha$) in refluxed pyridine solution. ^{13}C NMR (CD$_2$Cl$_2$, 298 K): δ_C, ppm 146.3 (C$_\alpha$), 145.0 (C$_\alpha$), 142.8 (C$_\alpha$), 126.4 (C$_\alpha$). MALDI-TOF MS: *m/z* 1410.68 (calcd. for ^{12}C$_{88}$^{13}C$_8$H$_{105}$N$_7$OP 1411.82).

Fe$^{\text{III}}$(TBP$_8$Cz)(^{13}C$_\alpha$). Insertion of iron was carried out by the addition of 20 equiv. of Fe$^{\text{III}}$(acac)$_3$ according to the Goldberg's method [41]. ^{13}C$_\alpha$-enriched complex was similarly prepared. MALDI-TOF MS: *m/z* 1419.82 (calcd. for ^{12}C$_{88}$^{13}C$_8$H$_{104}$FeN$_7$ 1419.69).

[Fe$^{\text{II}}$(TBP$_8$Pz)(tBuNC)$_2$]. To the CD$_2$Cl$_2$ solution of Fe$^{\text{III}}$(TBP$_8$Pz)I was added 3 equiv. of ^{t}BuNC. The spectrum immediately changed to form diamagnetic [Fe$^{\text{II}}$(TBP$_8$Pz)(^{t}BuNC)$_2$]. Similar reaction occurred in toluene-d$_8$ solution. ^{1}H NMR (toluene-d$_8$, 298 K): δ_H, ppm 8.62 (16H, o-H), 7.58 (16H, m-H), 1.46 (p-^{t}Bu), -0.78 (coord-^{t}BuNC). EPR spectrum taken for frozen CH$_2$Cl$_2$ solution at 4 K was silent.

(Bu$_4$N)$_2$[Fe$^{\text{II}}$(TBP$_8$Pz)(CN)$_2$]. To the toluene-d$_8$ solution of Fe$^{\text{III}}$(TBP$_8$Pz)I was added 5 equiv. of Bu$_4$N(CN). The ^{1}H NMR spectrum changed to give diamagnetic (Bu$_4$N)$_2$[Fe$^{\text{II}}$(TBP$_8$Pz)(CN)$_2$]. ^{1}H NMR (toluene-d$_8$, 298 K): δ_H, ppm 8.46 (16H, o-H), 7.57 (16H, m-H), 1.48 (p-^{t}Bu). *The chemical shift of 2.51 reported for p-^{t}Bu protons in our previous paper was mistyped and should be corrected to 1.48* [30].

RESULTS AND DISCUSSION

Spin state of four-, five, and six-coordinate iron(III) corrolazine complexes

By using the method developed by Goldberg and co-workers [41], we have obtained four-coordinate Fe$^{\text{III}}$(TBP$_8$Cz), five-coordinate [Fe$^{\text{III}}$(TBP$_8$Cz)(L)]*, and six-coordinate [Fe$^{\text{III}}$(TBP$_8$Cz)(L)$_2$]*. In the following section, we will report the spectroscopic and magnetic data of these complexes and discuss mainly the spin-state of these complexes.

UV-visible spectra

i) Addition of CN to Fe$^{\text{III}}$(TBP$_8$Cz). Figure 1(a) shows the UV-vis spectral change of Fe$^{\text{III}}$(TBP$_8$Cz) measured in CH$_2$Cl$_2$ solution at 298 K after the addition of 0–1.0 equiv. of tetrabutylammonium cyanide (Bu$_4$NCN). As the CN$^-$ ion was added, the absorption band at 433 nm showed a bathochromic shift to 437 nm. By the further addition of CN$^-$ up to 120 equiv., the band at 437 nm decreased and the new band at 477 nm increased in intensity as shown in Fig. 1(b). The results strongly indicate that the CN$^-$ ions bind to the iron(III) ions of Fe$^{\text{III}}$(TBP$_8$Cz) in a stepwise fashion to form firstly the mono-adduct (Bu$_4$N)-[Fe$^{\text{III}}$(TBP$_8$Cz)(CN)] with Soret band at 437 nm and then the bis-adduct (Bu$_4$N)$_2$[Fe$^{\text{III}}$(TBP$_8$Cz)(CN)$_2$] with Soret band at 477 nm.

ii) Addition of various ligands to Fe$^{\text{III}}$(TBP$_8$Cz). Other ligands such as HIm, DMAP, Py, 4-CNPy, and ^{t}BuNC were similarly added to the CH$_2$Cl$_2$ solutions of Fe$^{\text{III}}$(TBP$_8$Cz). The spectral change was similar to that of the CN$^-$ case; the Soret band showed a small bathochromic shift in each case. However, in contrast to the case of the cyanide addition, no further change was observed in UV-vis spectra even by the addition of larger excess of ligand. Figure 1(c) shows the UV-vis spectra observed when *ca.* 50 equiv. of the ligands were added to the CH$_2$Cl$_2$ solutions of Fe$^{\text{III}}$(TBP$_8$Cz). The spectra were

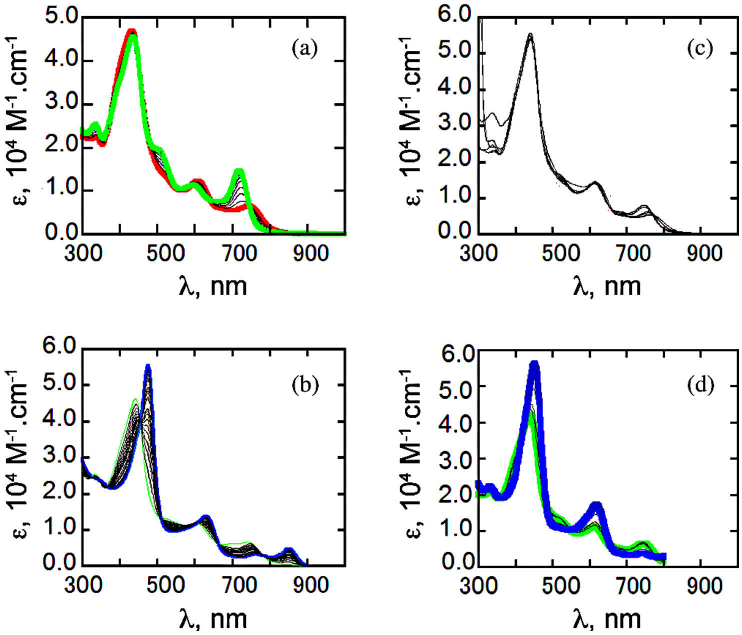

Fig. 1. UV-vis spectral change when (a) 0–1equiv and (b)1–120 equiv of Bu_4NCN was added to the CH_2Cl_2 solution of Fe^{III} (TBP_8Cz). Red, green, and blue lines show the UV-vis spectra of $Fe^{III}(TBP_8Cz)$, $(Bu_4N)[Fe^{III}(TBP_8Cz)(CN)]$, and $(Bu_4N)_2[Fe^{III}(TBP_8Cz)(CN)_2]$, respectively. (c) UV-vis spectra of $Fe^{III}(TBP_8Cz)$ measured after the addition of 50 equiv of ligands(L) such as Hlm, 1-MeIm, DMAP, Py, 4-CNPy, and ^{t}BuNC at ambient temperature. (d) UV-Vis spectra spectra at 298 and 213 K are shown in green and blue lines, respectively.

essentially the same as those obtained by the addition of 1.0 equiv. of the ligands. On the basis of these results, it is concluded that the complexes carrying HIm, 1-MeIm, DMAP, Py, 4-CNPy, and ^{t}BuNC maintain the five-coordinate structure at least at ambient temperature even in the presence of large amount of the ligand.

In order to see if six-coordinate complex can be formed at lower temperature, the UV-vis spectra of the CH_2Cl_2 solution of $Fe^{III}(TBP_8Cz)$ containing 1000 equiv. of HIm was examined. At ambient temperature, the spectrum was essentially the same as that obtained in the presence of 50 equiv. of HIm. As the temperature was lowered, however, the Soret band at 440 nm showed a bathochromic shift together with the Q-band at 614 nm as shown in Fig. 1(d). The presence of the isosbestic points is a clear indication that the spectral change corresponds to the conversion from five- to six-coordinate complex as the temperature is lowered. The absorption maxima of the bis-HIm complex were 451, 619, and 745 nm. Thus, the Soret band was by 26 nm shorter than that of the corresponding bis-CN complex.

^{1}H NMR spectra

i) Orbital consideration. DFT calculations revealed that corrolazine has closely located HOMO and HOMO-1 labeled as a_2 and b_1, respectively [47, 48]. Figure 2 shows the a_2 and b_1 HOMOs reported by Tangen and Ghosh for $Cu^{III}Cz$ [47]. Since the complex belongs to the C_{2v} group, the symmetries of the iron d_{xz} and d_{yz} orbitals, which are labeled as e_g in D_{4h} complex, are lowered to the b_1 and a_2, respectively. Thus, these orbitals can interact with the nearly degenerated corrolazine HOMO-1(b_1) and HOMO(a_2). In contrast, the iron d_{xy} orbital has b_2 symmetry and is therefore orthogonal to any of the corrolazine orbitals. The d_{xy} orbital could interact with some corrolazine orbitals if the corrolazine core deforms as frequently observed in porphyrin complexes. However, all the X-ray crystallographic analysis of corrolazine complexes reported previously exhibited the relatively planar structure [31, 32, 38–40]. Furthermore, recent theoretical study has also revealed that the parent corrole ring does not ruffle [49]. Taken together, it should be reasonable to suppose that the half-occupied d_{xy} orbital is orthogonal to any of the corrolazine π orbitals. Thus, if the complex exhibits large isotropically shifted signals, it should indicate that the complex has half-occupied iron d_{xz} and/or d_{yz} orbitals. Although the electron densities among the eight C_α and eight C_β atoms are not much different in the HOMO(a_2), they are quite inhomogeneous in the HOMO-1(b_1), *i.e.* two of the C_β and two of the C_α atoms have zero coefficients. Thus, we can expect a large spread of the isotropically shifted C_α, o-H, and m-H signals if the complex has half-occupied d_{xz} orbital. The ^{1}H and ^{13}C NMR spectra have to be interpreted on the basis of the orbital interactions mentioned here.

ii) $Fe^{III}(TBP_8Cz)$. Figure 3(a) shows the ^{1}H NMR spectra of $Fe^{III}(TBP_8Cz)$ taken in CD_2Cl_2 solution at 298 K. Poorly resolved signals appeared at 11–13 ppm together with the four broad signals at around 8 ppm; 7.5, 7.9, 8.2, and 8.8 ppm. Goldberg and co-workers confirmed that the complex adopts the intermediate-spin (S = 3/2)

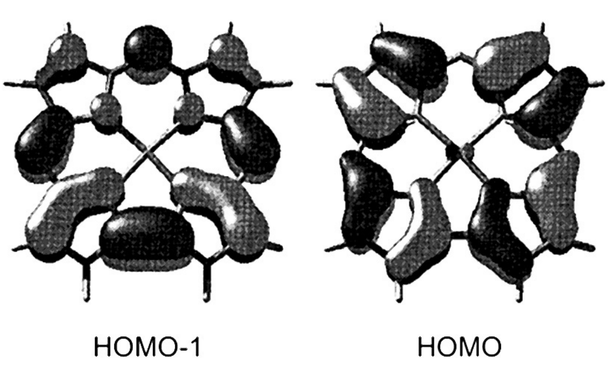

Fig. 2. The a_2 HOMO and b_1 HOMO-1 of $Cu^{III}Cz$ adapted from E. Tangen and A. Ghosh, *J. Am. Chem. Soc.* 2002, **124**, 8117–8121, with permission from the American Chemical Society.

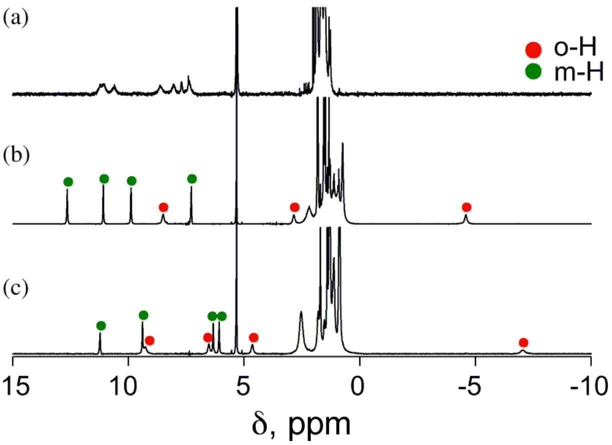

Fig. 3. ^{1}H NMR spectra of (a) Fe^{III}(TBP$_8$Cz), (b) (Bu$_4$N)-[Fe^{III}(TBP$_8$Cz)(CN)] and, (c) (Bu$_4$N)$_2$[Fe^{III}(TBP$_8$Cz)(CN)$_2$] taken in CD$_2$Cl$_2$ at 298 K. Red and green circles indicate the o-H and m-H signals, respectively.

state in frozen toluene solution at 77 K on the basis of the EPR spectrum; the $g_\perp$ and $g_\parallel$ values were determined to be 4 and 2.0, respectively [41]. As mentioned later, we have also confirmed by the Mössbauer spectra that the microcrystalline sample of Fe^{III}(TBP$_8$Cz) maintains the S = 3/2 spin state in the temperature range 77–295 K.

We and others reported that structurally analogous porphyrazine complexes such as Fe^{III}(TBP$_8$Pz)X adopt the S = 3/2 spin state if X is Cl$^-$, Br$^-$, or I$^-$ [30, 50, 51]. In the case of the iodide complex Fe^{III}(TBP$_8$Pz)I, the o-H and m-H signals were observed at 6.10 and 11.74 ppm, respectively [30]. The downfield shift of the m-H signal in Fe^{III}(TBP$_8$Pz)I is ascribed to the sizable amount of spin density on the pyrrole-C$_\beta$ atoms, which in turn indicates that the d$_{xz}$ and/or d$_{yz}$ orbitals are half-occupied. In the present case, the m-H signals at 11–13 ppm strongly indicate that Fe^{III}(TBP$_8$Cz) adopts the S = 3/2 spin state in CD$_2$Cl$_2$ solution at 298 K.

iii) Addition of CN- to Fe^{III}(TBP$_8$Cz). Figure 3(b) shows the ^{1}H NMR spectrum when 1.0 equiv. of Bu$_4$NCN was added to the CD$_2$Cl$_2$ solution of Fe^{III}(TBP$_8$Cz). The four sharp signals observed at 12.64, 11.08, 9.88, and 7.28 ppm at 298 K can be assigned to the m-H signals of (Bu$_4$N)[Fe^{III}(TBP$_8$Cz)(CN)]. The three broad o-H signals were observed at much more upfield positions; 8.50, 2.85, and -4.58 ppm. The chemical shift of the fourth signal, though hidden by the strong butyl signals of Bu$_4$NCN, was determined to be 2.07 ppm from the Curie plots. The COSY spectrum shown in Fig. S1(a) of the Supporting information exhibits the correlation peak between 12.64 and -4.58 ppm. Similarly, the m-H signals at 11.08, 9.88, and 7.28 ppm correlate with the o-H signals at 1.50, 2.85, and 8.50 ppm, respectively. Thus, the chemical shifts (ppm) of the (o-H, m-H) signals of four phenyl rings are (-4.58, 12.64), (1.50, 11.08), (2.85, 9.88), and (8.50, 7.28), which clearly indicates that the spin density at the C$_\beta$ atom mainly determines the chemical shifts of the phenyl protons. Namely, the C$_\beta$ atom having larger spin density induces more upfield and downfield shifts of the o-H and m-H signals, respectively. The average chemical shifts of the o-H and m-H signals were 2.07 and 10.22 ppm, respectively. The presence of the upfield shifted o-H and the downfield shifted m-H signals suggests that the S = 3/2 state is maintained during the addition of 1.0 equiv. of the CN$^-$ ion.

By the further addition of CN$^-$ to the mono-CN complex, four new signals appeared and increased their intensities. When 3.0 equiv. of CN$^-$ was added, the signals for the mono-CN complex completely disappeared and only the signals for bis-CN complex were observed as shown in Fig. 3(c). On going from the mono-CN to the bis-CN complex, the four m-H signals shifted upfield and appeared at 11.21, 9.39, 6.33, and 6.07 ppm. The four broad o-H signals also showed appreciable shifts and appeared at 9.28, 6.51, 4.64, and -7.00 ppm. As in the case of the mono-CN complex, the COSY spectrum given in Fig. S1(b) showed the correlation between the o-H and m-H signals at 4.64 and 9.39 ppm, 6.51 and 6.07 ppm, and 9.28 and 6.33 ppm. Although no correlation peak was observed between the o-H signal at -7.00 ppm and the m-H signal at 11.21 ppm, they should belong to the same phenyl ring. Thus, the average chemical shifts of the o-H and m-H signals changed from 2.07 and 10.22 ppm, respectively, in the mono-CN complex to 3.33 and 8.25 ppm, respectively, in the bis-CN complex. The results suggest that the spin densities on the C$_\beta$ atoms have decreased by the addition of the second CN$^-$ ion, which in turn indicates that the spin-state has changed from the S = 3/2 to the S = 1/2. Whether this complex adopts the $(d_{xy})^2(d_{xz}, d_{yz})^3$ or $(d_{xz}, d_{yz})^4(d_{xy})^1$ ground state will be discussed later.

Figure 4(a) shows the Curie plots of the m-H signals of [(TBP$_8$Cz)Fe^{III}(CN)]$^-$(green lines) and [(TBP$_8$Cz)-Fe^{III}(CN)$_2$]$^{2-}$(black lines). The averaged Curie slopes for the m-H signals were +770 and +230 ppm· K, respectively, while those of the o-H signals (not shown) were -2200 and -1400 ppm· K, respectively. The decrease in the absolute values of the Curie slopes on going from the mono-CN to the bis-CN complex again indicates that the spin densities on the C$_\beta$ atoms have decreased in this order and supports the change in spin-state from the S = 3/2 to the S = 1/2.

iv) Addition of various ligands to Fe^{III}(TBP$_8$Cz). Figure 4(a) also shows the Curie plots of the m-H signals (red symbols) of the complex obtained by the addition of 50 equiv. of HIm to the CD$_2$Cl$_2$ solutions of Fe^{III}(TBP$_8$Cz). The Curie plots showed curvature in the temperature range between 300 and 250 K. As the temperature was further lowered, the plots showed reasonably good linearity. The results can be explained in terms of the change in spin state from the five-coordinate S = 3/2 to the six-coordinate S = 1/2. Similar curvature was observed in the Curie plots of the DMAP complexes (red symbols) as shown in Fig. 4(b) though the curvature

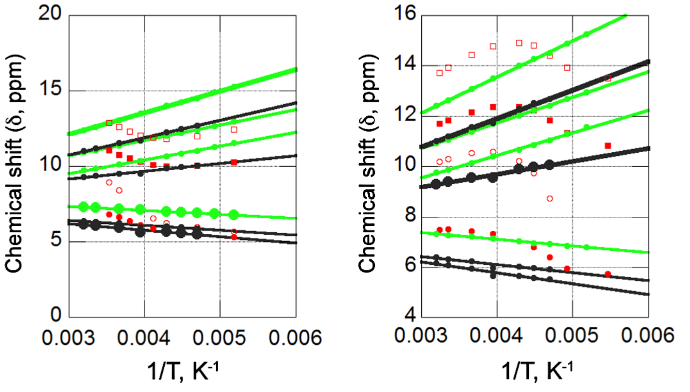

(a) (b)

Fig. 4. Curie plots of the m-H signals in $(Bu_4N)[Fe^{III}(TBP_8Cz)(CN)]$ (green lines) and $(Bu_4N)_2[Fe^{III}(TBP_8Cz)(CN)_2]$ (black lines) together with those of the complex obtained by the addition of 50 equiv of (a) Him (red symbols) and (b) DMAP (red symbols)

was observed at much lower temperature, *i.e.* below 250 K, as compared with the HIm complex. The Curie plots of the Py complex started to curve below 200 K as shown in Fig. S2. Thus, the change in spin state occurs at much lower temperature as the axial ligand changes from HIm to DMAP, and then to Py. In contrast, the 4-CNPy and ${}^tBuNC$ complexes shown also in Fig. S2 exhibited good straight line in the temperature range examined, *i.e.* 308–193 K, indicating that the complexes maintain the five-coordinate S = 3/2 spin state.

v) Chemical shifts. Table 1 shows the ${}^1H$ NMR chemical shifts of mono-CN and bis-CN complexes as well as those of $Fe^{III}(TBP_8Cz)$ taken in the presence of 50 equiv. of the ligands such as HIm, 1-MeIm, DMAP, Py, 4-CNPy, and ${}^tBuNC$ at 298 and 193 K. As is revealed from the Curie plots, all the complexes except for bis-CN adopt the five-coordinate S = 3/2 state at 298 K. Characteristic feature of the ${}^1H$ NMR spectra of the S = 3/2 complexes is the downfield shifts of three of the m-H signals; the fourth one appears quite close to the diamagnetic positions. In contrast, the bis-CN complex adopting the S = 1/2 at 298 K exhibit two of the m-H signals at the downfield positions; other two signals appear at slightly upfield positions. As the temperature is lowered to 193 K, the HIm, 1-MeIm, and DMAP complexes adopt the six-coordinate low-spin state as is revealed from the presence of two downfield shifted and two slightly upfield shifted m-H signals; the m-H chemical shifts of these complexes are quite close to those of the bis-CN complex. In contrast, the Py, 4-CNPy, and ${}^tBuNC$ complexes maintain the five-coordinate S = 3/2 state even at 193 K as is revealed by the similarity in chemical shifts to those of the mono-CN complex. Spin states of these complexes at 298 and 193 K are summarized in Table 1.

${}^{13}C$ NMR

Figure 5(a,b) shows the ${}^{13}C$ NMR spectra of ${}^{13}C_\alpha$-enriched five-coordinate $(Bu_4N)[Fe^{III}(TBP_8Cz)(CN)]$ and six-coordinate $(Bu_4N)_2[Fe^{III}(TBP_8Cz)(CN)_2]$ taken in CD_2Cl_2 solution at 298 K. For comparison, the ${}^{13}C$ NMR spectra of ${}^{13}C_\alpha$-enriched porphyrazine complexes such as $[Fe^{III}(TBP_8Pz)(I)]$ (298 K) and $(Bu_4N)[Fe^{III}(TBP_8Pz)(CN)_2]$ (273 K) taken in CD_2Cl_2 solution are also given in Figs 5(c) and 5(d), respectively [30].

Table 1. ${}^1H$ NMR chemical shifts of $[Fe^{III}(TBP_8Cz)(L)]^*$ and $[Fe^{III}(TBP_8Cz)(L)_2]^*$ at 298 and 193 K together with their spin state

Ligands	${}^1H$ NMR (298 K, CD_2Cl_2)						Spin state	${}^1H$ NMR (193 K, CD_2Cl_2)						Spin state
	o-H		m-H		${}^tBu$			o-H		m-H		${}^tBu$		
CN^-	8.50	2.85	12.64	11.08	1.82	1.80	S = 3/2	8.13	-0.83	15.27	12.96	1.89	1.83	S = 3/2
	1.50	-4.58	9.88	7.28	1.55	1.49		-3.31	-11.91	11.56	6.79	1.53	1.30	
$(CN^-)_2$	9.28	6.51	11.21	9.39	1.70	1.40	S = 1/2	10.15	5.27	13.26	10.31	1.67	1.30	S = 1/2
	4.64	-7.00	6.33	6.07	1.28	0.90		2.31	-14.82	5.73	5.26	1.20	0.54	
HIm	8.03	—	13.21	11.34	1.83	1.71	S = 3/2	9.74	—	12.44	10.29	1.60	1.19	S = 1/2
	0.28	-5.52	9.71	7.14	1.52	1.40		—	-11.56	5.68	5.31	1.08	0.51	
1-MeIm	8.75	—	13.18	11.22	1.86	1.80	S = 3/2	10.04	5.79	12.94	10.39	1.15	1.61	S = 1/2
	1.01	-6.12	9.22	—	1.52	1.45		—	-13.53	5.68	5.26	1.22	0.52	
DMAP	9.46	—	13.94	11.85	2.10	1.88	S = 3/2	9.41	—	13.74	11.10	1.35	1.66	S = 1/2(major)
	0.04	-6.02	10.31	7.51	1.68	1.62		0.78	-14.00	—	5.84	1.26	0.72	
Py	—	—	14.74	12.38	2.16	1.89	S = 3/2	9.22	0.88	17.04	13.68	2.16	1.89	S = 3/2(major)
	-1.25	-7.70	10.40	—	1.68	1.59		-4.48	-16.02	10.04	6.48	1.51	1.38	
4-CNPy	8.05	3.48	15.46	12.88	2.26	1.93	S = 3/2	8.25	-1.71	19.32	15.33	2.54	2.00	S = 3/2
	-2.36	-9.22	10.51	7.39	1.71	1.60		-7.56	-18.00	12.09	7.08	1.65	1.65	
${}^tBuNC$	10.01	—	14.83	12.44	2.15	1.89	S = 3/2	10.22	—	17.46	14.09	2.08	1.93	S = 3/2
	-1.41	-8.21	10.23	7.34	1.65	1.58		-5.31	-16.58	9.97	6.34	1.62	1.47	

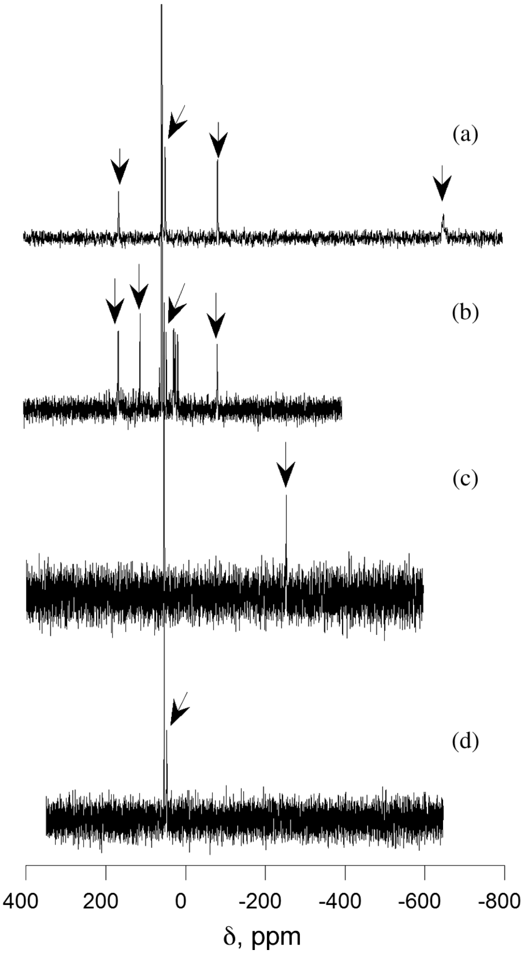

Fig. 5. ^{13}C NMR spectra of ^{13}C$_\alpha$-enriched (a) $(Bu_4N)[Fe^{III}(TBP_8Cz)\text{-}(CN)]$, (b) $(Bu_4N)_2[Fe^{III}(TBP_8Cz)(CN)_2]$, (c) $[Fe^{III}(TBP_8Pz)(I)]$ taken in CD_2Cl_2 solution at 298 K, and (d) $(Bu_4N)[Fe^{III}(TBP_8Pz)\text{-}(CN)_2]$ taken in CD_2Cl_2 solution at 273 K

The C$_\alpha$ signals of $(Bu_4N)_2[Fe^{III}(TBP_8Cz)(CN)_2]$ were widely spread; they appeared at 162, 50, -79, and -625 ppm. Similarly, the C$_\alpha$ signals of $(Bu_4N)_2[Fe^{III}(TBP_8Cz)\text{-}(CN)_2]$ were observed at 163, 105, 40, and -87 ppm. Thus, the average C$_\alpha$ chemical shifts of the mono- and bis-CN complexes were calculated to be -123 and 55 ppm, respectively. In the case of the porphyrazine complexes, the C$_\alpha$ chemical shift of the iodide complex with S = 3/2 was -252 ppm while that of the bis-CN complex with S = 1/2 was 53 ppm. These results clearly indicate that $(Bu_4N)\text{-}[Fe^{III}(TBP_8Cz)(CN)]$ and $(Bu_4N)_2[Fe^{III}(TBP_8Cz)\text{-}(CN)_2]$ adopt the S = 3/2 and S = 1/2, respectively [51, 52].

EPR spectra

Figure 6 shows the EPR spectra of the complexes obtained by the addition of 50 equiv. of a wide variety of ligands(L) to the toluene solutions of $Fe^{III}(TBP_8Cz)$. As is revealed by the UV-vis spectra at ambient temperature, only CN$^-$ ion binds the iron(III) of $Fe^{III}(TBP_8Cz)$ to form the bis-adduct; all the other ligands examined in this study bind the iron to form only the mono-adducts. EPR spectra taken in frozen toluene solution at 15 K exhibited the clearly separated rhombic type spectra for all the complexes examined, indicating the formation of six-coordinate low-spin $[Fe^{III}(TBP_8Cz)(L)_2]^*$. The g values of these complexes are listed in Table 2. The g values of the Py and DMAP complexes are essentially the same as those reported by Goldberg and co-workers [41].

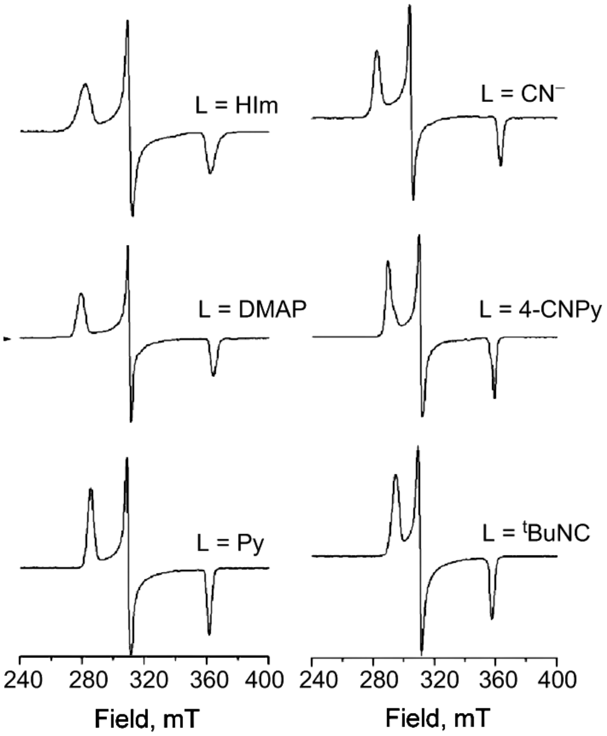

Fig. 6. EPR spectra of the samples consisting of $Fe^{III}(TBP_8Cz)$ and 50 equiv of various ligands(L) taken in frozen toluene solution at 15 K.

We have considered that the addition of much smaller amount of ligands(L) should form five-coordinate $Fe^{III}(TBP_8Cz)(L)$ at 15 K and that they exhibit the EPR spectra characteristic to the intermediate-spin state. However, the EPR spectra of $Fe^{III}(TBP_8Cz)$ taken in the presence of 3 equiv. of the ligands such as CN$^-$, HIm, and ^{t}BuNC showed the rhombic-type spectra that are the same to those shown in Fig. 6.

Table 2. EPR g values of $[Fe^{III}(TBP_8Cz)(L)_2]^*$ determined in frozen toluene solution at 15 K

Ligand (L)	g_1	g_2	g_3
HIm	2.47	2.21	1.89
1-MeIm	2.46	2.22	1.88
DMAP	2.48	2.22	1.89
CN$^-$	2.44	2.26	1.89
Py	2.40	2.22	1.90
4-CNPy	2.38	2.21	1.90
^{t}BuNC	2.36	2.21	1.92

In the case of the low-spin iron(III) complexes with axial symmetry(D_{4h} or C_{4v}), the EPR spectra can be classified into three categories [3]. The complex that adopts the $(d_{xy})^2(d_{xz}, d_{yz})^3$ ground state exhibits either the large g_{max} or the rhombic type spectrum depending on the orientation of the axial ligands. Thus, the low-spin complexes having either perpendicularly aligned planar ligands or linear ligands exhibit the large g_{max} type spectra, while the low spin complexes having parallel aligned planar ligands exhibit the rhombic type spectra. In contrast, the complex that adopts the $(d_{xz}, d_{yz})^4(d_{xy})^1$ ground state exhibits the axial type spectrum with $g_{\perp}$ value less than 2.6 [53]. In the present case, however, the rhombic type spectra are expected regardless of the electronic ground states because corrolazine does not possess C_4 axis perpendicular to the ring. Thus, we cannot determine the electronic ground state simply from the spectral type.

Mössbauer spectra

Figure 7 shows the Mössbauer spectra of (a) $Fe^{III}(TBP_8Cz)$ and (b) $(Bu_4N)_2[Fe^{III}(TBP_8Cz)(CN)_2]$ taken for the microcrystalline sample from 77 to 295 K (or 292 K in the latter complex). Tables S1 and S2 in the Supporting information list the Mössbauer parameters. In the case of $Fe^{III}(TBP_8Cz)$, the QS values were temperature independent and they were maintained at 3.91 mm s^{-1}. The large QS values together with the IS values of 0.45–0.56 mm s^{-1} strongly indicate that the complex adopts the S = 3/2 [54–57], as pointed out by Goldberg and co-workers on the basis of the EPR spectroscopy [41]. In the case of $(Bu_4N)_2[Fe^{III}(TBP_8Cz)(CN)_2]$, the IS values were 0.07–0.10 and QS values were 2.72–2.75 mm s^{-1}, though the QS values are slightly larger than the typical values for the low-spin complexes. The results could be interpreted in terms of the unsymmetrical coordination field caused by the triaza-corrole structure.

Effective magnetic moments

Effective magnetic moments of $Fe^{III}(TBP_8Cz)$ were measured by the Evans method in CD_2Cl_2 solution in the presence of 50 equiv. of each ligand [43]. As shown in Fig. 8(a), the effective magnetic moments of $(Bu_4N)_2[Fe^{III}(TBP_8Cz)(CN)_2]$ were 2.0 ± 0.1 μ_B in the temperature range 193–298 K. The results indicate that the complex maintains the S = 1/2 in CD_2Cl_2 solution. Consistent with the Curie plots in Fig. 4, both the DMAP and 1-MeIm complexes showed the conversion of spin state from the S = 3/2 to the S = 1/2 as the temperature is lowered, suggesting the change in structure from five- to six-coordination. In contrast, the 4-CNPy complex maintains the five-coordinate S = 3/2 structure even at 193 K as in the case of the mono-CN complex.

Figure 8(b) shows the temperature dependence of the effective magnetic moments of the mono-CN and bis-CN complexes measured for the microcrystalline samples at 4.5 to 300 K by SQUID magnetometry. The effective magnetic moments for the microcrystalline sample obtained from the solution containing $Fe^{III}(TBP_8Cz)$ and HIm (3 equiv.) is also given in Fig. 8(b). As expected, the mono-CN complex showed the effective magnetic moments expected for the S = 3/2 in the wide range of temperature. The bis-CN complex showed the low-spin state below 150 K. However, the effective magnetic moment of this complex increased gradually as the temperature was raised above 150 K and reached 2.42 μ_B at 300 K. The result suggests that the spin state partly changed to the S = 3/2 as the temperature was raised from 150 to 300 K. The result should be ascribed to the spin crossover phenomenon in the bis-CN complex rather than to the change in coordination structure from six- to five-coordinate complex in the solid state. In contrast to the solution data, the HIm complex maintained the S = 1/2 spin state in the temperature range examined. The result suggests that the bis(HIm) complex was crystallized preferentially from the solution containing $Fe^{III}(TBP_8Cz)$ and 3 equiv. HIm. Thus, the CD_2Cl_2 solution prepared from the microcrystalline sample used for the SQUID measurement showed the ^1H NMR signals indicative of the S = 3/2 spin state at ambient temperature due to the conversion from the six-coordinate to the five-coordinate complex in solution.

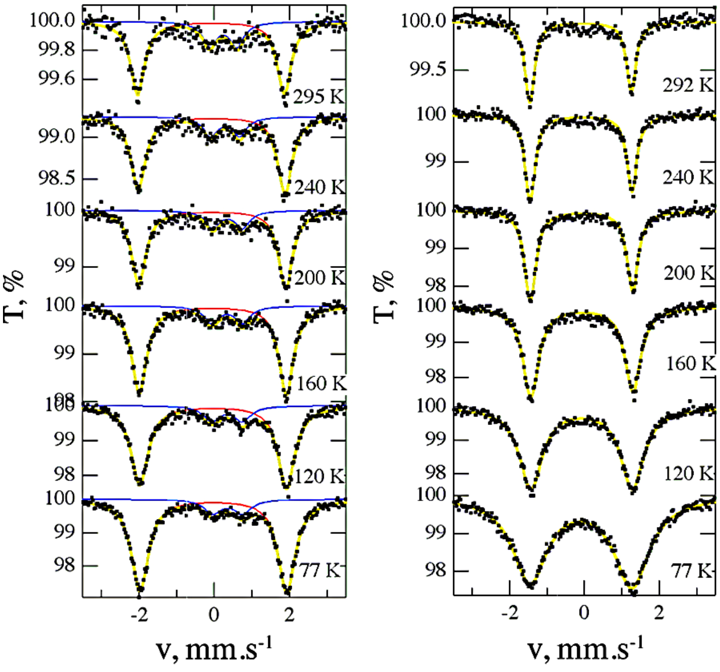

(a) (b)

Fig. 7. Mössbauer spectra of (a) $Fe^{III}(TBP_8Cz)$ and (b) $(Bu_4N)_2[Fe^{III}(TBP_8Cz)(CN)_2]$ taken for the microcrystalline samples.

Electron configurations of six-coordinate low-spin corrolazine complexes

In the previous section, we have discussed mainly the spin states of four-, five-, and six-coordinate corrolazine complexes on the basis of various spectroscopic and magnetic data. We now consider the electron configurations of the six-coordinate corrolazine complexes.

$(Bu_4N)_2[Fe^{III}(TBP_8Cz)(CN)_2]$. Among the six-coordinate corrolazine complexes examined in this study, the bis-CN complex $(Bu_4N)_2[Fe^{III}(TBP_8Cz)(CN)_2]$ has been most extensively studied. This is because the complex is easily formed by the addition of 3 equiv. of CN^- into the CH_2Cl_2 solutions of $Fe^{III}(TBP_8Cz)$ even at the ambient temperature.

As mentioned in the previous section, $(Bu_4N)_2[Fe^{III}(TBP_8Cz)(CN)_2]$ adopts mainly the $S = 1/2$ both in solution and in the solid state in a wide range of temperature on the basis of the EPR (frozen toluene solution, 15 K) and Mössbauer (solid, 77–295 K) spectroscopy as well as the magnetic susceptibility data obtained by the SQUID (solid, 4.5–300 K) and Evans method (CD_2Cl_2 solution, 213–313 K); the SQUID data has suggested a presence of small amount of the $S = 3/2$ complex at 300 K. The question is how to determine the electronic ground state of the low-spin complex.

If the corrolazine complexes adopt the $(d_{xy})^2(d_{xz}, d_{yz})^3$ ground state, the unpaired electron in the d_{xz} or d_{yz} orbital can interact with the corrolazine HOMO-1 or HOMO shown in Fig. 2. These interactions should increase the spin densities on the C_β atoms. Consequently, the o-H and m-H signals shift upfield and downfield, respectively. The large spread of these signals can be another good evidence for the $(d_{xy})^2(d_{xz}, d_{yz})^3$ ground state. If, on the other hand, the complex adopts the $(d_{xz}, d_{yz})^4(d_{xy})^1$ ground state, the unpaired electron in the d_{xy} orbital, which is labeled as b_2 in the six-coordinate complex with C_{2v} symmetry, has no suitable corrolazine orbitals to interact. Thus, every signal should appear quite close to its diamagnetic position.

As listed in Table 1, both the o-H and m-H signals of $(Bu_4N)_2[Fe^{III}(TBP_8Cz)(CN)_2]$ showed large spread, *i.e.* the amounts of the spread for the o-H and m-H signals were 16.28 and 5.14 ppm, respectively, at 298 K. The result indicates that the spin densities of the peripheral C_β atoms are quite inhomogeneous, which can be explained if the d_{xz} orbital is half-occupied. In addition, the C_α signals of the bis-CN complex also spread widely, *i.e.* from -87 to +163 ppm. These results strongly indicate that the bis-CN complex adopts the $(d_{xy})^2(d_{xz}, d_{yz})^3$ ground state.

$[Fe^{III}(TBP_8Cz)(L)_2]^*$. Complexes carrying HIm, 1-MeIm, and DMAP adopt the six-coordinate low-spin state only at the low temperature as revealed by the temperature dependence of the effective magnetic moments shown in Fig. 8 and the ^{1}H NMR chemical shifts listed in Table 1. The similarity of the ^{1}H NMR chemical shifts to those of the bis-CN complex suggests that these complexes also adopt the $(d_{xy})^2(d_{xz}, d_{yz})^3$ ground state.

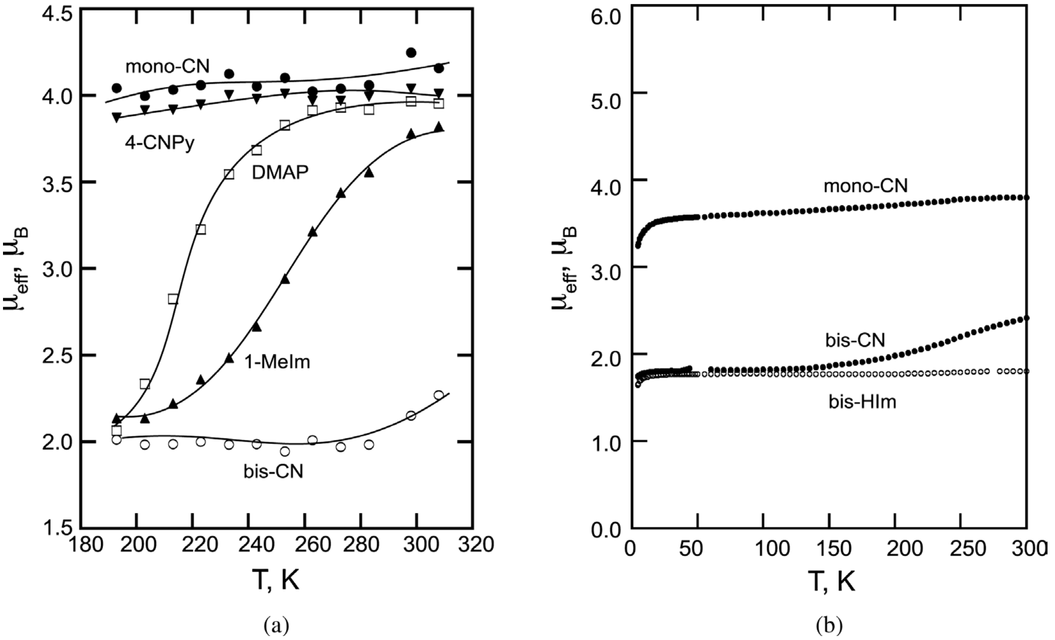

(a) (b)

Fig. 8. (a) Effective magnetic moments of $Fe^{III}(TBP_8Cz)$ determined by the Evans method in the presence of 50 equiv of CN^-, 1-MeIm, DMAP, and 4-CNPy in CD_2Cl_2 solution. Mono-CN complex $(Bu_4N)[Fe^{III}(TBP_8Cz)(CN)]$ is obtained by the addition of 1.0 equiv of $Bu_4N(CN)$ to the CD_2Cl_2 solution of $Fe^{III}(TBP_8Cz)$. (b) Temperature dependence of the effective magnetic moments determined by the SQUID magnetometry for the microcrystalline samples of $(Bu_4N)_2[Fe^{III}(TBP_8Cz)(CN)_2]$, $(Bu_4N)[Fe^{III}(TBP_8Cz)$-$(CN)]$, and $[Fe^{III}(TBP_8Cz)(Him)_2]$

The amounts of the spread of the o-H signals reached as much as 21.12, 23.66, and 23.41 ppm for the HIm, 1-MeIm, and DMAP complexes, respectively, at 193 K.

Complexes carrying Py, 4-CNPy, and ^{t}BuNC form the low-spin bis-adducts only at extremely low temperature as confirmed by the EPR spectra taken in frozen toluene solution at 15 K. The rhombic EPR spectra clearly indicates that these complexes are in the S = 1/2 state. In the absence of the NMR data, it is very difficult to conclude whether the complex adopts the $(d_{xy})^2(d_{xz}, d_{yz})^3$ or $(d_{xz}, d_{yz})^4(d_{xy})^1$ ground state. We speculated that these complexes should also adopt the $(d_{xy})^2(d_{xz}, d_{yz})^3$ ground state because the EPR spectrum of each complex is quite similar to that of the bis-CN complex. For example, the g values of the bis-^{t}BuNC complex were 2.36, 2.21, and 1.92, which are close to those of the bis-CN complex, *i.e.* 2.44, 2.26, and 1.89. As mentioned in the Introduction, low-spin bis-^{t}BuNC complexes almost always adopt the $(d_{xz}, d_{yz})^4(d_{xy})^1$ ground state because ^{t}BuNC has low-lying π^* orbital and stabilizes the d_π orbitals. The exceptional complexes showing the $(d_{xy})^2(d_{xz}, d_{yz})^3$ ground state are 1 and 2 having one and two nitrogen atoms at the *meso*-positions, respectively, as shown in Chart 1 [26, 27]. Thus, it seems to be a reasonable assumption to consider that $[Fe^{III}(TBP_8Cz)({}^{t}BuNC)_2]$ having three nitrogen atoms at the *meso*-positions of the corrole structure adopts the $(d_{xy})^2(d_{xz}, d_{yz})^3$ ground state.

Comparison of the electronic structures with those of porphyrazine complexes

In the previous paper, we have reported that the low-spin porphyrazine complex, $(Bu_4N)[Fe^{III}(TBP_8Pz)(CN)_2]$, adopts the $(d_{xy})^2(d_{xz}, d_{yz})^3$ ground state on the basis of the large g_{max} type signal in EPR, the upfield shift of the C_α signal in ^{13}C NMR, and the downfield shifted m-H signal in ^{1}H NMR spectra [30]. Thus, the electronic ground state of $(Bu_4N)_2[Fe^{III}(TBP_8Cz)(CN)_2]$ is the same as that of $(Bu_4N)[Fe^{III}(TBP_8Pz)(CN)_2]$ as far as the solvent is CH_2Cl_2.

In toluene solution, however, the porphyrazine complex exhibited a completely different NMR spectra. The o-H and m-H signals appeared at 8.46 and 7.57 ppm, respectively. Similarly, the C_α signal appeared at 151 ppm. These chemical shifts are quite close to those of the diamagnetic complexes. Furthermore, the EPR spectrum was silent at 4.2 K. Thus, the complex is not paramagnetic $(Bu_4N)[Fe^{III}(TBP_8Pz)(CN)_2]$ but diamagnetic $(Bu_4N)_2[Fe^{II}(TBP_8Pz)(CN)_2]$, indicating that the porphyrazine core is more easily reduced than the corresponding corrolazine core especially in toluene solution.

As mentioned, the bis-^{t}BuNC complex of corrolazine, $[Fe^{III}(TBP_8Cz)({}^{t}BuNC)_2]$, was formed only when the temperature was lowered to 15 K as revealed by the EPR spectrum taken in frozen toluene solution. In the case of the porphyrazine complex, however, the addition of excess amount of ^{t}BuNC to the CD_2Cl_2 (or toluene-d_8) solution of $Fe^{III}(TBP_8Pz)Cl$ led to the formation of the bis-^{t}BuNC complex even at the ambient temperature. However, the ^{1}H NMR spectrum has revealed that the complex is diamagnetic $[Fe^{II}(TBP_8Pz)({}^{t}BuNC)_2]$; the chemical shifts for the o-H, m-H and ^{t}Bu-H were determined to be 8.62, 7.58, and 1.59 ppm, respectively, which are quite close to those of diamagnetic $[Fe^{II}(TBP_8Pz)(CN)_2]$ mentioned above. The ^{13}C NMR spectrum of the complex obtained from ${}^{13}C_\alpha$-enriched $Fe^{III}(TBP_8Pz)Cl$ exhibited the C_α signal at the diamagnetic position in CD_2Cl_2 solution, *i.e.* 151 ppm. The diamagnetic nature was further confirmed by the EPR spectrum, which showed no signal in frozen CH_2Cl_2 solution at 4 K. These results suggest that the iron(III) ion in $Fe^{III}(TBP_8Pz)Cl$ was reduced to iron(II) in the presence of excess amount of ^{t}BuNC to form low-spin diamagnetic $[Fe^{II}(TBP_8Pz)\ ({}^{t}BuNC)_2]$.

Facile reduction of $Fe^{III}(TBP_8Pz)Cl$ in the presence of excess CN^- (in toluene) and ^{t}BuNC (both in toluene and CH_2Cl_2) to form diamagnetic $[Fe^{II}(TBP_8Pz)(CN)_2]$ and $[Fe^{II}(TBP_8Pz)({}^{t}BuNC)_2]$, respectively, suggests that $Fe^{III}(TBP_8Pz)Cl$ is much more easily reduced than $Fe^{III}(TBP_8Cz)$, which should be one of the major differences between these two ring systems.

CONCLUSION

Spin states and electron configurations of four-, five- and six-coordinate corrolazine complexes have been examined. In CH_2Cl_2 (or CD_2Cl_2) solution, the spectroscopic data have unambiguously shown that the five-coordinate $[Fe^{III}(TBP_8Cz)(L)]^*$ (L = CN^-, HIm, 1-MeIm, DMAP, Py, 4-CNPy, and ^{t}BuNC) adopt the S = 3/2 spin state at ambient temperature. As for the six-coordinate cyanide complex, $(Bu_4N)_2[Fe^{III}(TBP_8Cz)(CN)_2]$, the spectroscopic and magnetic data have shown that the complex adopts the S = 1/2 both in solution and in the solid in a wide range of temperature; the population of the S = 3/2 increases slightly as the temperature is raised. The large spread of the o-H, m-H, and pyrrole C_α signals in the ^{1}H and ^{13}C NMR spectra has indicated that the complex adopts the $(d_{xy})^2(d_{xz}, d_{yz})^3$ electronic ground state. Other six-coordinate $[Fe^{III}(TBP_8Cz)(L)_2]$ (L = HIm, 1-MeIm, and DMAP), which are the major components at least below 200 K, also adopt the low-spin $(d_{xy})^2(d_{xz}, d_{yz})^3$ ground state. Thus, the electronic structure of six-coordinate corrolazine complexes is similar to that of the porphyrazine bis-CN complex $[(TBP_8Pz)Fe^{III}(CN)_2]^-$. In toluene solution, however, some differences are observed between corrolazine and porphyrazine complexes. The addition of excess amount of CN^- and ^{t}BuNC to the toluene solutions of $Fe^{III}(TBP_8Pz)Cl$ has led to the formation of diamagnetic $[Fe^{II}(TBP_8Pz)(CN)_2]^{2-}$ and $[Fe^{II}(TBP_8Pz)({}^{t}BuNC)_2]^-$. These results suggest that the iron(III) ion of the porphyrazine complex is much more easily reduced than that of the corresponding corrolazine complex.

Acknowledgements

This work was supported by the Grant-in-Aid for Scientific Research from the Ministry of Education, Culture, Sports, Science and Technology, Japan (Grant 22750052 to T.I. and Grant 22550157 to M.N.). Thanks are due to the Research Center for Molecular-Scale Nanoscience, the Institute for Molecular Science (IMS). This work was also supported by the Research Center for Materials with Integrated Properties, Toho University.

Supporting information

COSY spectra and Mössbauer parameters (Figs S1–S2 and Tables S1–S2) are given in the supplementary material. This material is available free of charge *via* the Internet at http://www.worldscinet.com/jpp/jpp.shtml.

REFERENCES

‡ Abbreviations: TBP$_8$Cz: trianion of 2,3,7,8,12,13,17,18-octakis(4-*tert*-butylphenyl)corrolazine, TBP$_8$Pz: dianion of 2,3,7,8,12,13,17,18-octakis-(4-*tert*-butyl-phenyl)porphyrazine, MAzP: dianion of 2,3,7,8,12,13,17,18-octaethyl-5-azaporphyrin, DAzP: dianion of 2,8,12,18-tetrabutyl-3,7,13,17-tetramethyl-5,15-diazaporphyrin, HIm: imidazole, 1-MeIm: 1-methylimidazole, DMAP: 4-(N,N-dimethylamino)pyridine, Py: pyridine, 4-CNPy: 4-cyanopyridine, ^{t}BuNC: *tert*-butylisocyanide.

1. Nakamura M. *Coord. Chem. Review.* 2006; **250**: 2271–2294.
2. Nakamura M, Ohgo Y and Ikezaki A. *Handbook of Porphyrin Science*, Vol. 7, Kadish KM, Smith KM and Guilard R. (Eds.) World Scientific: Singapore, 2010; pp 1–146.
3. Walker FA. *The Porphyrin Handbook*, Vol. 5, Kadish KM, Smith KM and Guilard R. (Eds.) Academic Press: San Diego, 2000; pp 81–183.
4. Evans DR and Reed CA. *J. Am. Chem. Soc*. 2000; **122**: 4660–4667.
5. Sakai T, Ohgo Y, Ikeue T, Takahashi M and Nakamura M. *J. Am. Chem. Soc*. 2003; **125**: 13028–13029.
6. Cheng R-J, Wang Y-K, Chen P-Y, Han Y-P and Chang C-C. *Chem. Commun*. 2005; 1312–1314.
7. Ling Y and Zhang Y. *J. Am. Chem. Soc*. 2009; **131**: 6386–6388.
8. Ikezaki A, Ohgo Y, Watanabe T and Nakamura M. *Inorg. Chem. Commun*. 2008; **11**: 1199–1202.
9. Neya S, Ohgo Y, Nakamura M and Funasaki N. *Bull. Chem. Soc. Jpn*. 2000; **73**: 2759–2765.
10. Ikeue T, Ohgo Y, Takahashi M, Takeda M, Neya S, Funasaki N and Nakamura M. *Inorg. Chem*. 2001; **40**: 3650–3652.
11. Ohgo Y, Neya S, Ikeue T, Funasaki N, Takahashi M, Takeda M and Nakamura M. *Inorg. Chem.* 2002; **41**: 4627–4629.
12. Ohgo Y, Neya S, Takahashi M, Takeda M, Funasaki N and Nakamura M. *Chem. Lett*. 2003; **32**: 526–527.
13. Sessler JL, Gebauer A and Vogel E. *The Porphyrin Handbook*, Vol. 2, Kadish KM, Smith KM and Guilard R. (Eds.) Academic Press: San Diego, 2000; pp 1–54.
14. Vogel E, Köcher M, Schmickler H and Lex J. *Angew. Chem. Int. Ed. Engl*. 1986; **25**: 257–259.
15. Vogel E, Balci M, Pramod K, Koch P, Lex J and Ermer O. *Angew. Chem. Int. Ed. Engl*. 1987; **26**: 928–931.
16. Wehrle B, Limbach H-H, Kocher M, Ermer O and Vogel E. *Angew. Chem. Int. Ed. Engl*. 1987; **26**: 934–936.
17. Sessler JL, Brucker EA, Weghorn SJ, Kisters M, Schafer M, Lex J and Vogel E. *Angew. Chem. Int. Ed. Engl*. 1994; **33**: 2308–2312.
18. Aukauloo MA and Guilard R. *New J. Chem*. 1994; **18**: 1205–1207.
19. Callot HJ, Rohrer R and Tschamber T. *New J. Chem*. 1995; **19**: 155–159.
20. Vogel E, Broring M, Scholz P, Deponte R, Lex J, Schmickler H, Schaffner K, Braslavsky SE, Muller M, Porting S, Weghorn SJ, Fowler CJ and Sessler JL. *Angew. Chem. Int. Ed. Engl*. 1997; **36**: 1651–1654.
21. Waluk L. *Handbook of Porphyrin Science*, Vol. 7, Kadish KM, Smith KM and Guilard R. (Eds.) World Scientific: Singapore, 2010; pp 359–435.
22. Kobeissi M, Toupet L and Simonneaux G. *Inorg. Chem*. 2001; **40**: 4494–4499.
23. Astashkin AV, Raitsimring AM and Walker FA. *J. Am. Chem. Soc.* 2001; **123**: 1905–1913.
24. Cai S, Lichtenberger L and Walker FA. *Inorg. Chem.* 2005; **44**: 1890–1903.
25. Ikezaki A, Nakamura M, Juillard S and Simonneaux G. *Inorg. Chem*. 2006; **45**: 6728–6739.
26. Nakamura K, Ikezaki A, Ohgo Y, Ikeue T, Neya S and Nakamura M. *Inorg. Chem.* 2008; **47**: 10299–10307.
27. Ohgo Y, Neya S, Uekusa H and Nakamura M. *Chem. Commun.* 2006; 4590–4592.
28. Simonneaux G, Hindre F and Le Plouzennec M. *Inorg. Chem*. 1989; **28**: 823–825.
29. Simonneaux G, Schunemann V, Morice C, Carel L, Toupet L, Winkler H, Trautwein AX and Walker FA. *J. Am. Chem. Soc*. 2000; **122**: 4366–4377.
30. Ikeue T, Kurahashi S, Handa M, Sugimori T and Nakamura M. *J. Porphyrins. Phthalocyanines* 2008; **12**: 1041–1049.
31. Ramdhanie B, Stern CL and Goldberg DP. *J. Am. Chem. S*oc. 2001; **123**: 9447–9448.
32. Ramdhanie B, Zakharov LN, Reingold AL and Goldberg DP. *Inorg. Chem.* 2002; **41**: 4105–4107.
33. Mandimutsira BS, Ramdhanie B, Todd RC, Wang H, Zareba AA, Czernuszewicz RS and Goldberg DP. *J. Am. Chem. S*oc. 2002; **124**: 15170–15171.

34. Wang SH, Mandimutsira BS, Todd R, Ramdhanie B, Fox JP and Goldberg DP. *J. Am. Chem. Soc*. 2004; **126**: 18–19.
35. Grybo DT, Fox JP and Goldberg DP. *J. Porphyrins Phthalocyanines* 2004; **8**: 1091–1105.
36. Kerber WD and Goldberg DP. *J. Inorg. Biochem*. 2006; **100**: 838–857.
37. Lansky DE and Goldberg DP. *Inorg. Chem.* 2006; **45**: 5119–5125.
38. Lansky DE, Kosack JR, Narducci Sarjeant AA and Goldberg DP. *Inorg. Chem.* 2006; **45**: 8477–8479.
39. Lansky DE, Narducci Sarjeant AA and Goldberg DP. *Angew. Chem. Int. Ed.* 2006; **45**: 8214–8217.
40. Kerber WD and Goldberg DP. *J. Inorg. Biochem.* 2006; **100**: 838–857.
41. Kerber WD, Ramdhanie B and Goldberg DP. *Angew. Chem. Int. Ed.* 2007; **46**: 3718–3721.
42. McGown AJ, Kerber WD, Fujii H and Goldberg DP. *J. Am. Chem. Soc*. 2009; **131**: 8040–8048.
43. Evans DF and James TA. *J. Chem. Soc*. 1979; 723–726.
44. Groves JT, Quinn R, McMurry TJ, Nakamura M, Lang G and Boso B. *J. Am. Chem. Soc.* 1985; **107**: 354–360.
45. Nie H, Barret AGM and Hoffman BM. *J. Org. Chem.* 1999; **64**: 6791–6796.
46. Fox JP, Ramdhanie B, Zareba AA, Czemuszewicz RS and Goldberg DP. *Inorg. Chem.* 2004; **43**: 6600–6608.
47. Tangen E and Ghosh A. *J. Am. Chem. Soc*. 2002; **124**: 8117–8121.
48. Kobayashi N, Yokoyama M, Muranaka A and Ceulemans A. *Tetrahedron Lett*. 2004; **45**: 1755–1758.
49. Thomas KE, Conradie J, Hansen LK and Ghosh A. *Inorg. Chem*. 2011; **50**: 3247–3251.
50. Fitzgerald JP, Haggerty BS, Rheingold AL, May L and Brewer GA. *Inorg. Chem*. 1992; **31**: 2006–2013.
51. Stuzhin PA, Hamdush M and Ziener U. *Inorg. Chim. Acta* 1995; **236**: 131–139.
52. Ikeue T, Ohgo Y, Saitoh T, Yamaguchi T and Nakamura M. *Inorg. Chem*. 2001; **40**: 3423–3434.
53. Ikeue T, Ohgo Y, Saitoh T, Nakamura M, Fujii H and Yokoyama M. *J. Am. Chem. Soc.* 2000; **122**: 4068–4076.
54. Reed CA and Guiset F. *J. Am. Chem. Soc*. 1996; **118**: 3281–3282.
55. Ikeue T, Saitoh S, Yamaguchi T, Ohgo Y, Nakamura M, Takahashi M and Takeda M. *Chem. Commun*. 2000; 1989–1990.
56. Debrunner P. *Iron Porphyrins* (part 3), Lever ABP and Gray HB. (Eds.) VCH: Weinheim, 1983; pp 139–234.
57. Gütlich P and Ensling J. *Inorganic Electronic Structure and Spectroscopy*, Solomon EI and Lever ABP. (Eds.) Wiley: New York, 1999; pp 161–211.